

## Article

# On the Use of Modern Engineering Codes for Designing a Small Wind Turbine: An Annotated Case Study

Francesco Papi , Alberto Nocentini, Giovanni Ferrara  and Alessandro Bianchini \* 

Department of Industrial Engineering, Università Degli Studi di Firenze, via di Santa Marta 3, 50139 Firenze, Italy; fr.papi@unifi.it (F.P.); alberto.nocentini@stud.unifi.it (A.N.); giovanni.ferrara@unifi.it (G.F.)  
\* Correspondence: alessandro.bianchini@unifi.it

**Abstract:** While most wind energy comes from large utility-scale machines, small wind turbines (SWTs) can still play a role in off-grid installations or in the context of distributed production and smart energy systems. Over the years, these small machines have not received the same level of aerodynamic refinement of their larger counterparts, resulting in a notably lower efficiency and, therefore, a higher cost per installed kilowatt. In an effort to reduce this gap during the design of a new SWT, the scope of the study was twofold. First, it aimed to show how to combine and best exploit the modern engineering methods and codes available in order to provide the scientific and industrial community with an annotated procedure for a full preliminary design process. Secondly, special focus was put on the regulation methods, which are often some of the critical points of a real design. A dedicated sensitivity analysis for a proper setting is provided, both for the pitch-to-feather and the stall regulation methods. In particular, it is shown that stall regulation (which is usually preferred in SWTs) may be a cost-effective and simple solution, but it can require significant aerodynamic compromises and results in a lower annual energy output in respect to a turbine making use of modern stall-regulation strategies. Results of the selected case study showed how an increase in annual energy production (AEP) of over 12% can be achieved by a proper aerodynamic optimization coupled with pitch-to-feather regulation with respect to a conventional approach.

**Keywords:** wind turbine; pitch; stall; aerodynamics; engineering codes



**Citation:** Papi, F.; Nocentini, A.; Ferrara, G.; Bianchini, A. On the Use of Modern Engineering Codes for Designing a Small Wind Turbine: An Annotated Case Study. *Energies* **2021**, *14*, 1013. <https://doi.org/10.3390/en14041013>

Academic Editor: David Wood  
Received: 13 January 2021  
Accepted: 10 February 2021  
Published: 15 February 2021

**Publisher's Note:** MDPI stays neutral with regard to jurisdictional claims in published maps and institutional affiliations.



**Copyright:** © 2021 by the authors. Licensee MDPI, Basel, Switzerland. This article is an open access article distributed under the terms and conditions of the Creative Commons Attribution (CC BY) license (<https://creativecommons.org/licenses/by/4.0/>).

## 1. Introduction

To fulfill global energy needs, manufacturers and most of the wind turbine industry have concentrated their efforts on large utility-scale machines [1]. The standard design for horizontal-axis turbines consists of a three-blade, upwind rotor featuring an active yaw and pitch regulation. Such machines benefit from large levels of aerodynamic optimization, often using purposely developed airfoils featuring twisted and tapered blades and large resources for development and testing. On the other hand, small wind turbines (SWTs) often do not feature the same level of optimization, with low power coefficients often resulting from unoptimized designs [2]. Such sub-optimal aerodynamic designs have been identified amongst the issues that hamper the diffusion and economic feasibility of SWTs [3,4], with larger SWTs suffering the most from the often used simplistic approaches [4]. This type of turbine, which marked the dawn of wind energy, is still used in a variety of applications, from rural areas to off-grid applications [5]; notwithstanding this, their high levelized cost of energy [6] has thus far hampered an effective diffusion. On the other hand, interest has been rising lately again, as testified by the creation of a dedicated technical committee for SWTs by the European Academy of Wind Energy (EAWE) [7]; this is mainly due to the role that distributed production, even with small rated power, could have in the transition towards smart energy systems [8]. In doing so, the “old generation” of turbines seems unsuitable in terms of efficiency and flexibility, and so better designs are about to be explored.

The present article aimed to analyze the main issues causing low power output in an SWT while also detailing how an effective preliminary design can be achieved by using and properly integrating current industry best-practices and open-source tools. In particular, even though the latter are indeed familiar to the wind energy community, their conscious use is not trivial, and organic design guidelines are often not available. Effectively and economically designing an SWT is not a trivial task, and many hurdles must be overcome in terms of aerodynamics, materials, structural resistance, and economics.

While a good overview of these issues can be found in [4], the aim of the present study was twofold. On the one hand, it aspired to provide the reader with an organic overview of the steps that need to be followed for a first turbine design, suggesting how to integrate existing engineering open-source tools and how to tune them, especially in cases of the realistic turbulent inflow conditions that are required by standards (summarized in the chart in Appendix A). This, while not completely novel from a scientific point of view, is thought to be of industrial relevance and significance for newcomers. Guidelines and general indications on blade design can be in fact found in the available literature [9,10]. For instance, various aspects of aerodynamic design and optimization were discussed in [11]. Such studies, however, do not account for control or dynamic inflow conditions [12]. The study instead specifically focused on the implication of control for small wind turbines. In particular, it is shown that using modern control strategies, which have rarely been applied to SWTs, can lead to much more efficient design and more convenient loading. The importance of making an early decision regarding control in the design phase was assessed, as this aspect significantly influences aerodynamic design, and controller tuning and optimization should go hand in hand with aerodynamic optimization. Most small wind turbines indeed use a stall as their main power-limiting strategy. This involves controlling the rotor speed so that, as the wind speed increases, the turbine gradually enters the stall, the lift decreases, and the drag increases, thus effectively regulating the power output. Fixed-speed stall-controlled turbines were the de-facto standard in the nineties [2], and successful applications of this design can be found [13]; however, most stall-regulated turbines, including commercially available products, now feature variable speed generators [14]. By adopting variable-speed control, a turbine is able to operate at or near the design tip-speed ratio (TSR) at a low wind speed, greatly improving energy capture. Even when adopting variable speed control, however, significant compromises must be made in order to ensure good stall regulation, from setting the blades to a manual fixed pitch angle to varying the twist and chord distributions of the blade. Such compromises can be avoided if pitch regulation is employed. Two kinds of pitch regulation strategies are possible: pitch-to-stall and pitch-to-feather. As noted in [15], the pitch-to-stall strategy is able to provide effective regulation, though it increases most design loads. Moreover, given that the pitch-to-feather strategy is the most widely adopted control method in modern utility-scale turbines, this kind of pitch regulation is discussed in this paper. While the benefits of this control strategy are apparent, it does not come without drawbacks, mainly connected to its added complexity and, especially, cost. However, examples of manufacturers proposing this kind of solution can be found, as is the case with the line of products by Tozzi Nord [16]. For all of these reasons combined, two SWT designs are compared in this paper—a variable-speed stall-regulated turbine and a variable-speed, pitch-regulated turbine.

The selected testcase for the entire analysis was a 50 kW machine with a 200 m<sup>2</sup> swept rotor area, which is in line with the definition of an SWT according to International Electrotechnical Commission (IEC) 61400-2 [12]. The authors indeed had a direct industrial experience with this size of machine, and this experience mainly drove the present study. Due to the industrial non-disclosure agreement with the partner, however, all analyses were repeated on a purely theoretical case study. Notwithstanding this, the results are fully representative of those found in reality.

## 2. Methods

In this section, the numerical tools used throughout the study are briefly presented. The methods to determine a preliminary chord and twist distribution are explained. Then, the airfoils considered in the design process are discussed, and the modifications done to the ideal design in order to meet the desired targets in terms of power output are analyzed in detail.

### 2.1. Numerical Tools

The aerodynamic design process described in the previous sections was conducted using open-source, industry-standard computational tools. It is worth pointing out again that these methods are indeed not novel and well-known to the scientific community. Additionally, they have been extensively validated on a many study cases, both of small and utility-scale wind turbines, assessing their suitability for the scope. However, while approaching the industrial design of a new SWT, the authors found that detailed guidelines on how to consciously, organically, and in an integrated fashion use these methods were missing. On these bases, this study would like to represent a support to the industrial and scientific community in an overall attempt of improving the future design of this class of machines. A brief overview of the tools used in the study is provided in this paragraph.

Lift and drag airfoil characteristics were obtained with XFOil [17]. The tool is based on an inviscid panel method, and it has been used in the design of a vast amount of airfoils for all sorts of engineering uses, including the families used herein [18]. Even though a recent study pointed out that this method may have some issues in case of low Reynolds numbers and high angles of attack [19], its use in horizontal-axis rotors from the present power output and above can be considered as a solid choice, especially for the first design of blades, when multiple design variations need to be compared quickly.

For the present study, the characteristics were calculated using 200 panels per airfoil and setting a trailing edge gap of 2%. A Reynolds number of  $1 \times 10^6$  was used. The boundary layer transition was calculated with the  $N_{crit}$ -based shear layer transition method [20], and a value of  $N_{crit} = 9$  was used. The Reynolds number matched the final operating  $Re$  number fairly well, ranging between  $0.8 \times 10^6$  and  $1.3 \times 10^6$  depending on operating conditions, and was therefore considered acceptable; however, if this is not the case, a few design iterations might be required to ensure that lift and drag polars were suitable for the test case. The full-blade aerodynamic design was conducted in OpenFAST [21]. This open-source modular tool was developed by the National Renewable Energy Laboratory (NREL) and can model the full response of wind turbines, accounting for a wide variety of effects such as aerodynamics, elastodynamics, control-dynamics, and, for offshore installations, hydrodynamics. The code has been widely adopted, validated, and used in the design of multiple, industry-standard, reference wind turbines [22,23]. In the present study, only the aerodynamic and control-dynamics perspectives were explored in detail. The aerodynamic module AeroDyn [24] allows for the simulation of dynamic inflow conditions in the presence of atmospheric turbulence. Blade element momentum (BEM)-based aerodynamics also include corrections for wind shear, yaw misalignment, tip and hub losses, and tower-shadow effects. Dynamic stall is treated with the Beddoes–Leishman dynamic stall model included in AeroDyn. This correction is especially relevant for a stall-operated turbine operating in turbulent conditions. The turbine controller was integrated through the ServoDyn module. For the pitch-controlled turbine, an external routine was used, as detailed in the next section.

### 2.2. Ideal Blade Shape

A tentative blade design could be determined using BEM theory. A detailed explanation of the equations and their derivation can be found in [9], as only the aspects relative to

blade design are briefly presented herein. By manipulating BEM equations to express the power coefficient for each radial section without considering drag [9], one gets:

$$C_P(r) = \frac{8}{\lambda^2} \lambda_r^3 a' (1 - a) \quad (1)$$

The equation can be rearranged and written in terms of the flow angle  $\varphi$ :

$$C_P(r, \lambda, \varphi) = \frac{8}{\lambda^2} \sin^2 \varphi (\cos \varphi - \lambda_r \sin \varphi) (\sin \varphi + \lambda_r \cos \varphi) \lambda_r^2 \quad (2)$$

The flow angle distribution along the span that maximizes the power coefficient ( $C_P$ ) can be found by setting the partial derivative of Equation (2) equal to zero:

$$\frac{\partial}{\partial \varphi} (C_P(r, \lambda, \varphi)) = 0 \quad (3)$$

Solving Equation (3), one then gets:

$$\varphi = \frac{2}{3} \tan^{-1} \left( \frac{r}{R} \lambda \right) \quad (4)$$

The local blade twist can be calculated based on the flow angle as:

$$\gamma = \varphi - \theta - \alpha_{des} \quad (5)$$

where  $\theta$  is the blade pitch angle and  $\alpha_{des}$  is the local design angle of attack. The local blade chord can also be expressed as [9]:

$$c = \frac{8\pi r}{BC_l} (1 - \cos \varphi) \quad (6)$$

The twist and chord distributions obtained from Equations (5) and (6) do not account for drag and tip losses, and so the design angle of attack  $\alpha_{des}$  should be selected as the angle of attack that maximizes the glide ratio of the airfoil employed at the selected local radius. As shown in [10], when the airfoil glide ratio exceeds 40, the assumption of neglecting drag can be reasonably assumed. Moreover, the proposed design method determines the ideal blade shape in design conditions, with set tip-speed ratio (TSR) and pitch angle. It is then apparent that the design conditions should be chosen carefully. Rather than choosing the rotor and wind speed at rated conditions, a sounder choice would be to choose operating conditions based on the design wind speed distribution. In the present test case, a design wind speed of 8.5 m/s was chosen as the mean wind speed of a class IIA wind speed distribution. Another good choice could be the mode of the wind speed distribution. When designing a fixed-speed wind turbine, the mode of the wind speed distribution (i.e., the most frequent wind speed) should be chosen as a design point in order to ensure the turbine is operating at its design TSR most of the time. A variable speed wind turbine, on the other hand, can vary rotor speed to maintain a nominal TSR as wind speed varies, and the mean wind speed is therefore also a good choice because it ensures that the rotor speed is closer to the nominal value at the design point. The design TSR must also be chosen carefully, as this will contribute to determining rotor speed. Modern rotors generally operate between TSRs of 4 and 10 [25]. Higher tip-speed ratios decrease blade solidity and increase aerodynamic noise [26,27]. Therefore, based on these considerations and similar existing turbine designs [14,28–30], a medium-low TSR of 5.7 was selected here.

### 2.3. Airfoil Families

In order to obtain smooth chord and twist distributions, airfoils from the same family must be used along the entire blade. Several airfoil families have been designed specifically for wind turbines over the years by laboratories, scientists, and technical institutions such

as NREL (USA), Risø (Denmark), and Delft (The Netherlands). [18,31–33]. The selection of the required airfoils plays a crucial role in the aerodynamic design process. The shape of the selected airfoils is a compromise between performance, regulation characteristics (especially important in stall-regulated wind turbines), and structural stiffness. The mid and outer sections of a wind turbine blade are typically optimized for high aerodynamic performance, while the inner sections are designed to provide the required structural integrity and stiffness for the blade. Suggesting a family of airfoils is definitely not an easy task, since any of them have specific benefits and drawbacks that may be relevant to each different application; also, companies sometimes are willing to design proprietary airfoils tailored for their machine. However, the scope of the present work was to show how, even in case where one selects a very well-known family of “standard” airfoils, effective turbine designs can be achieved. In detail, research into airfoil families that would be suitable for a 50 kW wind turbine with a rotor diameter of 16 m led to the selection of two different airfoil families belonging to the S800 group developed and tested by NREL [18] for medium-size turbines rated at 20–150 kW with blades from 5 to 10 m in length, which was the size category of our interest.

The first family considered (Figure 1a) [18,34], with thin tip airfoils, was designed in 1987 and includes the S805A, S806A, S807, and S808 airfoils. This airfoil family was designed to have a low tip maximum lift coefficient ( $Cl_{max}$ ) (1.0) for a Reynolds number just over  $1 \cdot 10^6$ , and it is suitable for stall-regulated blades. The “A” designation stands for an improved version of an airfoil, based on wind-tunnel test results for a similar airfoil.

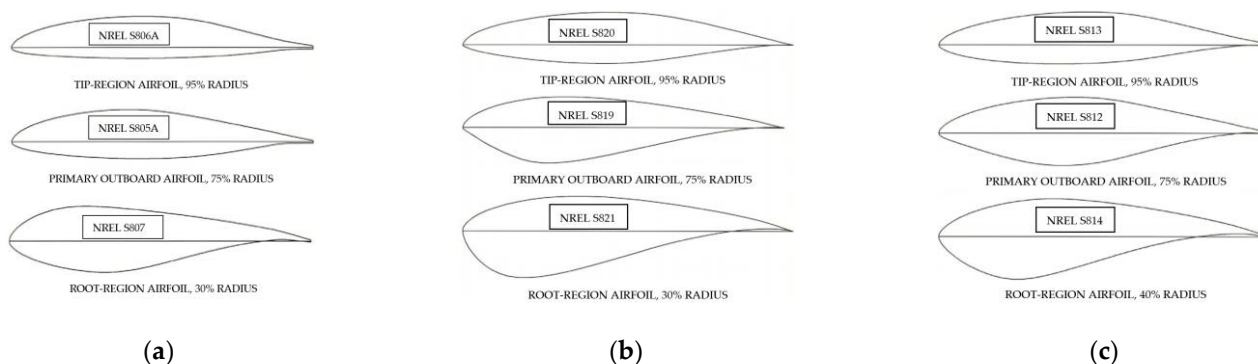


**Figure 1.** (a) Thin-airfoil family for medium blades (low tip  $Cl_{max}$ ), (b) thick-airfoil family for medium blades (low tip  $Cl_{max}$ ), (c) thick-airfoil family for large blades (low tip  $Cl_{max}$ ).

The second family (Figure 1b) [18,35], having thick tip airfoils, was designed in 1993 and consists of the S819, S820, and S821 airfoils. This family was designed to have performance characteristics similar to the previous family. The greater tip-region thickness helps accommodate overspeed-control mechanisms for stall-regulated rotors at the expense of a slightly higher drag [36,37]. Though these mechanisms are not used in modern turbines and were thus not included in this case study, the increased thickness is structurally beneficial. The S821 blade-root airfoil was designed to have restrained maximum lift coefficients, and have low profile-drag coefficients, and to be as insensitive as possible to roughness.

The low design lift coefficient of these airfoil families is indeed a design trait [33,36,38]. Specifically, on an SWT, the operating Reynolds number must be as high as possible to achieve the best aerodynamic performance. Based on Equation (6), decreasing the design lift coefficient implies an increase of the chord size required to reach a certain performance level. In turn, this increases the operating Reynolds number, which helps to lower drag and increase the glide ratio of the blade [10].

Finally, the S812, S813, and S814 (Figure 1c) [18,39–41] airfoil family was designed for large rotors rated at 100–400 kW with blades 10–15 m in length. Though this family of airfoils did not seem to fit the specification of the test case, it has been used successfully on

the Atlantic Orient AOC 15/50 three-bladed wind turbine. The designation 15/50 refers to the 15 m diameter rotor and its rated output of 50 kW [18,28,42]. This rated output is achieved at 12 m/s by the 50 Hz version and at 11.3 m/s by the 60 Hz version. This airfoil family was therefore also taken into consideration.

#### 2.4. Preliminary Performance Curves

Following the steps to determine the blade design presented in Section 2.1, the first steady analyses on OpenFAST for the three airfoil families were carried out. The focus in this phase was put on the stall-regulated turbine, as in this case, the aerodynamic design also influenced the regulation characteristics. As discussed previously, the design point was chosen to be 8.5 m/s, which is the mean wind speed of a class IIA (see Table 1).

**Table 1.** Turbine specifications. IEC: International Electrotechnical Commission.

| Parameter                 | Value           |
|---------------------------|-----------------|
| IEC wind class            | IIA             |
| Rotation axis             | Horizontal      |
| Number of blades          | 3               |
| Rotor diameter            | 16 m            |
| Hub radius                | 0.5 m           |
| Rated Power               | 50 kW           |
| Cut-in/cut-out wind speed | 2–20 m/s        |
| Rated wind speed          | 12 m/s          |
| Hub height                | 20.5 m          |
| Airfoil family            | NREL S821-19-20 |

Figure 2 shows the aerodynamic power produced as a function of the wind speed. These power curves were obtained without stall delay correction, and—only afterward once the most promising design was chosen—were the polars 3D-corrected and further refinements done (see Section 2.5). The regulation method for this preliminary design was variable speed stall regulation. In particular, the powers produced at 12 m/s were as follows: 50.4 kW for the S819–21 family, 52.6 kW for the S812–14 family, and 52.1 for the S805–8 family.

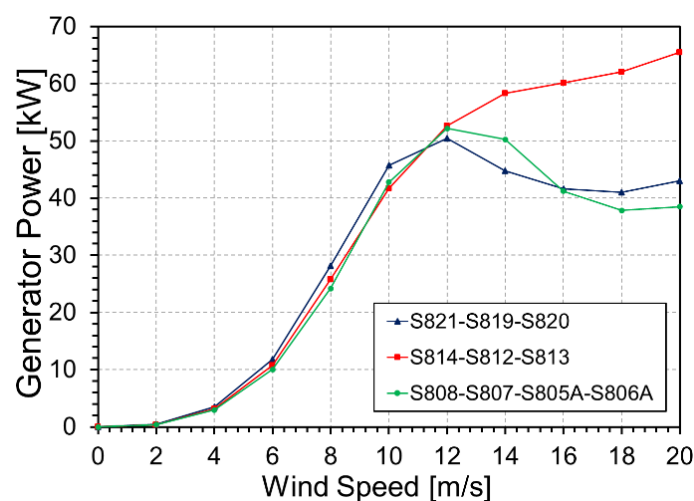


**Figure 2.** Turbine curves of generator power from the steady simulations in OpenFAST. Maximum rotor speed was set to 60 rpm.

Upon examination of the performance comparison in terms of power output, one could notice that the S821, S819, and S820 family was preferable to the others. In fact, it allowed us to reach the set power target of 50 kW at 12 m/s with good stall regulation, and it generated more power for below-rated wind speeds than the S805, S806, S807, and S808 family. The main preliminary characteristics of the turbine after the first preliminary design phase are shown in Table 1.

### 2.5. Modifications to Ideal Design

The ideal blade design seen so far did not account for various practical aspects that have to be considered in a real design [43]. The ideal blade first needs to be tapered at the tip. In this area, tip losses, which are not considered during preliminary design, would greatly decrease the energy extracted at blade tip [19,38]. In the present study, the tip region was tapered from 95% blade span outwards empirically. Since BEM methods were used in the present preliminary design study, although Prandtl's tip and hub-loss corrections were included in this work, accurate tip-loss evaluation was not possible and the influence of different tapering strategies was hard to assess. In fact, despite the fact that BEM methods are able to capture the primary effects of blade tapering by resolving blade-chord variations, the chord variations at the blade tip also influence tip-vortex strength and, as a consequence, blade loading. While some tip-loss correction models are somewhat sensible for tip chord distribution [44], Prandtl's model is not [24]. Moreover, while these corrections may be more sophisticated, they remain unlinked to the underlying physics; therefore, to properly study the effects of this phenomena, more sophisticated aerodynamic models are required. Decreasing the chord at the tip region also decreases aerodynamic loading, which is beneficial from a load standpoint and has little aerodynamic penalty due to the presence of the aforementioned tip-losses.

The blade also needs to be tapered at the blade root, where it is connected to the rotor hub. In this area, the local tip-speed ratio is very low, the local radius is short, and the produced torque is thus very low. On this basis, it is common practice to taper a blade empirically.

The lift and drag coefficients used throughout the blade must also be corrected to account for 3D flow effects. 3D effects were first noted by Himmelskamp [45] and tend to greatly increase the high-angle of attack lift of the inboard sections of a rotating blade [46]. These effects are present in rotating blades and although the underlying physics are not fully understood to this day, they seem to be caused by complex flow interactions in the boundary layer. In practical terms, radial pressure nonuniformities along the rotor blade create radial flow patterns, which have the main effect of delaying the stall. A brief explanation of the phenomena, as well as additional references, can be found in Chapter 3 of [10]. In the present study, the model proposed by Bak [47] was adopted and suggested. This model corrects both the lift and drag coefficients, and it can be relatively easily applied as an empirical correction step before the aerodynamic simulations are performed. The inclusion of 3D-effects was found to have a notable impact on turbine performance, especially for the stall-regulated turbine, as shown in Figure 3. Power was found to vary quite noticeably. At 12 m/s, the blades with a fixed  $-6.5^\circ$  pitch angle produced 49.4 kW (3D) and 48.4 kW (2D), while the blades with a  $-5^\circ$  pitch angle produced 50.4 kW (2D) and 59.8 kW (3D).

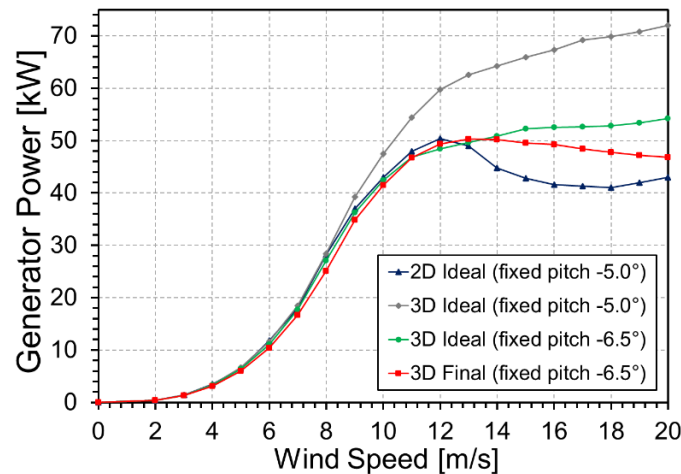


**Figure 3.** Generator power as a function of wind speed for the stall-regulated ideal blade design with 2D lift and drag coefficients, the ideal design with 3D effects, and the final design with 3D effects.

For this reason, the fixed blade pitch of the stall-regulated turbine was further tuned, and the twist of the inboard sections of the blade, which are most affected by stall delay, were modified to ensure the desired regulation characteristics, as shown in Figure 4. Reducing the twist angle increases the angle of attack, therefore pushing this part of the blade towards the stall. In fact, the angle of attack can be found from the flow angle  $\varphi$ , twist angle  $\delta$ , and pitch angle  $\theta$  as:

$$\alpha = \varphi - \delta - \theta \quad (7)$$

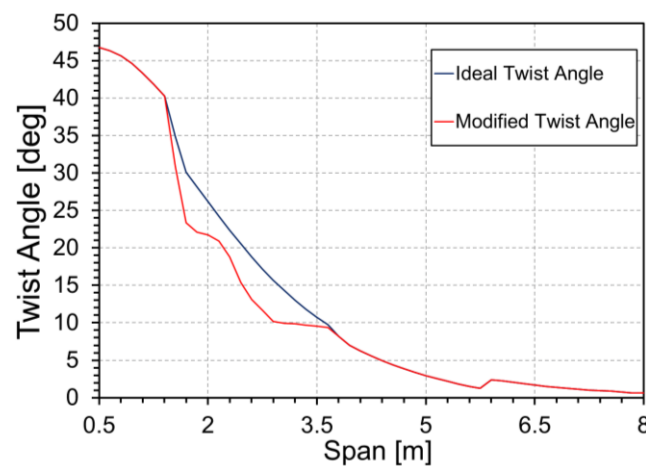


**Figure 4.** Changes to the optimal twist distribution to ensure good stall regulation.

Therefore, reducing the twist angle increases angle of attack, although it should be noted that changing blade twist influences axial and tangential induction, therefore changing the induced velocities and affecting the flow angle in Equation (7). The overall trend, however, remains valid, although some trial and error might be necessary. In other words, changing the twist angle can be seen as partial compensation for the stall delay effect, which, in contrast and as the name suggests, tends to delay the point of the stall, thus negatively affecting the blade's regulation capacity.

### 3. Turbine Control

In this section, the two adopted regulation methods, as well as the benefits and possible drawbacks of each solution, are explained in detail. This is probably the key element of the study since modern control strategies were often not applied to SWTs in the past. Throughout this paper, however, it will be proven that their use can be largely beneficial also in these rotors, leading to more effective designs.

#### 3.1. Pitch Control

Blade pitch control as a means of power curtailment is the modern control method, adopted on all utility-scale wind turbines. While two methods of pitch control are available, i.e., pitch-to-stall and pitch-to-feather, only the latter is used because it allows for much lower out-of-plane loads at high wind speeds.

The open-source NREL ROSCO controller [48] was used for this test case and is suggested as a valuable tool for a first analysis. The variable-speed pitch controller was developed based on the work of Mulders et al. [49], and it is able to regulate generator torque and blade pitch. It also allows for yaw control and individual pitch control (IPC).

Below the rated wind speed, a blade pitch is kept constant at fine pitch; in this case, it was set to  $0^\circ$ . The generator torque is calculated as in Equation (8):

$$\tau_g = K\omega_g^2 \quad (8)$$

where  $\omega_g$  is the generator speed. As also shown in [50], this simple formula is the result of the fact that in order to ensure maximum performance, the turbine must operate at peak  $C_p$  for all below-rated wind speeds. In the absence of pitch control, not active in this region,  $C_p$  is a function of the tip-speed-ratio alone that must therefore be kept constant. Therefore, as the theoretical available power is proportional to the cube of the wind speed, the generated power must be proportional to the cube of the rotor speed. The power maximizing the generator's torque constant (Equation (9)) can be calculated as [48]:

$$K = \frac{\rho\pi R^5 C_p}{2\lambda^3 N_g} \quad (9)$$

where  $N_g$  is the generator drive ratio. The relation can be easily derived from the expression of the rotor power coefficient by imposing generator torque, as in Equation (8).

Above rated power, the generator torque is fixed to the design torque  $\tau_g = P_r/\omega_r$  and the blade pitch is controlled with a Proportional-Integral (PI) controller (Equation (10)):

$$\Delta\theta(t) = K_p\Delta\omega_g(t) + K_i \int \Delta\omega_g dt \quad (10)$$

where  $\theta$  is the blade pitch. The proportional and integral gains  $K_p$  and  $K_i$ , respectively, depend on the blade pitch angle; in particular, as the blade pitch increases, rotor speed variations are more sensitive to small pitch variations. PI control in Equation (10) is derived from a more general Proportional-Integral-Derivative (PID) control strategy with the derivative term (D-term) set to zero. This is common practice in wind turbine pitch controllers. In most cases, the controller is able to adequately control rotor speed without the D-term, making controller tuning easier because there is one less parameter to tune. Furthermore, the D-term is very sensitive to high frequency fluctuations of the rotor speed, and an ill-chosen D-term could therefore introduce instability in a controller. Traditional tuning techniques involve the linearization of the system around an operating point to find controller gains. The linearization procedure must be repeated several times in the operating range. Alternatively, various authors have proposed methods to empirically calculate the gains [51].

In the present test case, the open-source ROSCO toolbox [52] was used to tune the controller. The gains were analytically calculated and depended on the design natural frequency  $\omega_{des}$  and damping ratio  $\zeta_{des}$ . In general, increased values of  $\omega_{des}$  decrease rotor

speed response time, while increased values of  $\zeta_{des}$  decrease the amount of rotor speed overshoot. For the present test case, the values of 0.82 and 1.4 were empirically selected for  $\omega_{des}$  and  $\zeta_{des}$ , respectively. These values were substantially higher than those found in much larger reference wind turbines, where values of  $\omega_{des}$  of 0.2–0.3 and  $\zeta_{des}$  of 0.7–0.9 are common [16,42] and are needed to effectively regulate a small wind turbine with low rotor inertia. As noted in [48], there is a limit to how fast rotor speed can be controlled (how high  $\omega_{des}$  can be) without incurring in erratic blade pitch behavior, and the value of 0.82 adopted for this case was found to be at the upper limit of this range. The controller response was tested with wind-step simulations below at and above rated speeds, as well as in turbulent wind. While response to turbulent wind is discussed in the following section, response to wind increments of 2 m/s are shown in Figure 5. The erratic blade pitch behavior can be clearly seen at 300 and 350 s.

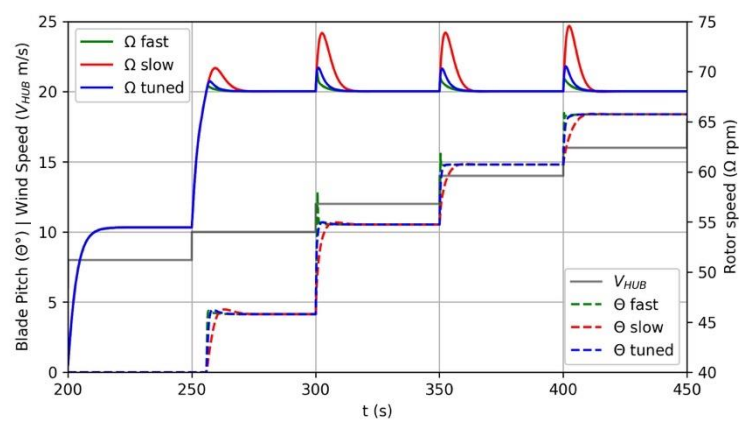


**Figure 5.** Turbine response to step-wind profiles for different values of controller natural frequency and damping ratio. Design natural frequency ( $\omega_{des}$ ) = 0.82 and damping ratio ( $\zeta_{des}$ ) = 1.4 for the tuned case,  $\omega_{des}$  = 1.2 and  $\zeta_{des}$  = 2 for the “fast” case, and  $\omega_{des}$  = 0.4 and  $\zeta_{des}$  = 0.8 for the “slow” case. Values for the “slow” case were still greater than those typically employed on utility-scale machines.

### 3.2. Stall Control

In this section, a variable-speed, stall-regulated strategy that eliminates the need for ancillary aerodynamic control systems is evaluated.

The variable-speed operation of wind turbines presents certain advantages over constant speed operation [50,53]. The primary advantage claimed for variable-speed turbines is the increased energy capture during partial load operation. Variable-speed operation allows the turbine to operate at near optimum  $C_p$  and to maximize power over a range of wind speeds. Moreover, variable-speed wind turbines use the inertia of the rotating mechanical parts of the system as a flywheel; this helps to smooth power fluctuations and reduces the drive train mechanical stress. Secondary benefits are acoustic signature and power quality [51]. The control logic is described in detail in [54], but the main details are explained herein as regulation strategy that significantly influences turbine regulation and, consequently, aerodynamic choices.

Typical variable-speed wind turbines have different regions of operation, as shown in Figure 5, where the generator torque as a function of the generator speed is shown. The turbine startup occurs in region 1, where the generator torque is zero. Once the generator speed has reached cut-in speed and power is produced normally, the turbine is operating in region 2. In this region, the generator torque control is used to vary the speed of the turbine to maintain the constant TSR corresponding to optimum  $C_p$ , thus maximizing the energy capture. In region 2, the torque curve is calculated as in Equation (7) and intersects the rated torque at a rotor speed that is significantly higher than the rated speed. It would of course be beneficial to operate the turbine on region 2 at an optimum  $C_p$  curve up to where

it intersects the rated torque, but the operation of the turbine at these high rotor speeds would result in a high blade tip speed and unacceptable noise emissions [31]. Therefore, a transition region is included between regions 2 and 3 (region  $2\frac{1}{2}$ ). Region  $2\frac{1}{2}$  depends linearly on rotor speed, starting at a rotor speed lower than the rated speed  $\omega_1$  and reaching the rated torque at, or slightly below, the rated speed  $\omega_2$ . The generator torque for this region can be expressed as Equation (11):

$$\tau_g(\omega) = \tau_1 + \frac{\tau_{rated} - \tau_1}{\omega_2 - \omega_1}(\omega - \omega_1) \quad (11)$$

where  $\omega$  is rotor speed,  $\tau_1$  is the generator torque at the rotor speed in which this region starts ( $\omega_1$ ),  $\tau_{rated}$  is rated torque, and  $\omega_2$  is the rotor speed at which we reach rated torque. Above the rated speed, the generator torque is set equal to the rated torque  $\tau_{rated}$ .

In region 3, generator torque is simply held constant at rated torque (see Figure 6).

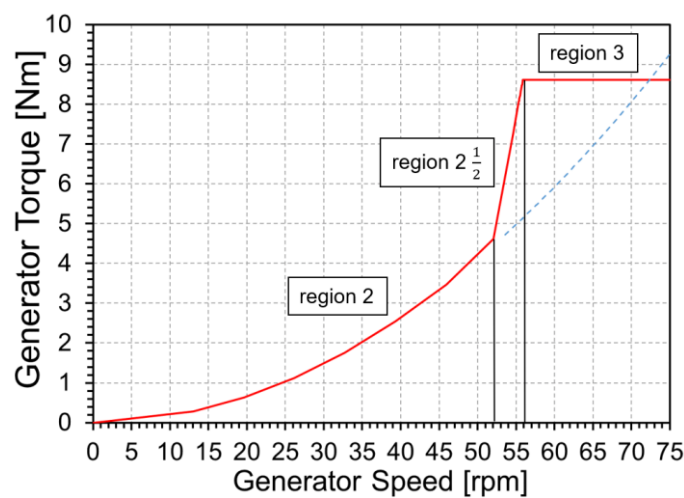


Figure 6. Variable-speed turbine operating regions.

Adequately tuning the slope and position of region  $2\frac{1}{2}$  ensures effective turbine regulation. Through region  $2\frac{1}{2}$ , the turbine is controlled to limit its rotational speed and, consequently, output power. In fact, limiting rotor speed decreases the TSR and forces the rotor into an aerodynamically stalled condition. This is usually called the “soft-stall” approach because it allows for the introduction of rather benign stall characteristics for the purposes of controlling maximum power.

### 3.3. Control Input Parameters

In Table 2, the main parameters used to set the torque-control strategy of the two turbines are shown. These are a result of a (in most cases) necessary sensitivity analysis. This paragraph hopefully helps the interested reader understand the influence of some of the main control parameters and how they can be tuned to reach the desired turbine performance. A baseline for these control parameters can be determined using the methods detailed in Sections 3.1 and 3.2. Several common techniques to ensure that power is correctly regulated using both control schemes were adopted for this study. The rated rotational speed of the stall-regulated turbine (i.e., the beginning of region 3 in Figure 6) was limited to 60 rpm because the turbine was designed to operate at a nominal TSR at 8.5 m/s wind speed and to enter off-design conditions as wind speed increases to force the blade to stall and the power to be regulated. Therefore, to effectively regulate power with a stall control scheme, the turbine needs to be forced to enter off-design conditions before the rated wind speed. A nominal rotor speed for the pitch-regulated turbine was chosen so that the design TSR could be maintained up to 10 m/s wind speed. The high value of rated generator torque for the stall-regulated turbine was set to avoid rotor overspeed in high

wind speed turbulent scenarios. In practice, this means that, even at a rated power, the turbine would operate in region  $2\frac{1}{2}$ . Operating in this region would ensure that the rotor does not speed-up as a response to steep wind speed increases. On the contrary, if the rotor is allowed to speed-up, the TSR and, consequently, the power increase, causing the rotor to quickly become uncontrolled and reach its terminal velocity. This also highlights the importance of considering dynamic inflow conditions early on in the design stage. Finally, the value of  $K$  (Equation (8)), was different in the two cases because the peak  $C_P$  design TSR were different for the two turbines.

**Table 2.** OpenFAST variable-speed generator model inputs.

| Parameter                       | Stall-Regulation          | Pitch-Regulation          |
|---------------------------------|---------------------------|---------------------------|
| Rated generator speed           | 60 rpm                    | 68 rpm                    |
| Rated generator torque          | 12,878.58 Nm              | 7727.02 Nm                |
| $K$ (see Equation (7))          | 1.645 Nm/rpm <sup>2</sup> | 1.694 Nm/rpm <sup>2</sup> |
| Slip % in region $2\frac{1}{2}$ | 26%                       | n/a                       |

#### 4. Simulation Set-Up

Once preliminary steady-state performance curves are obtained, it is important to account for more realistic environmental cases early in the design process. The reasons are twofold: first, it is important to assess turbine behavior in dynamic conditions, and secondly, the turbine will have to be certified in the later stages of the design process. For instance, as mentioned previously, it is crucial to verify that adequate turbine control is achieved in dynamic conditions. Moreover, the design loads calculated by simulating the turbine in dynamic environmental conditions can be used as a base for preliminary structural design. Here, the turbine was simulated in a normal power production situation, corresponding to the IEC Design Load Cases (DLCs) 1.2 [12]. The chosen turbine class was class IIA. This represents a class of turbines designed for medium wind speed (W.S.) and high turbulence sites.

One hundred fourteen 10-min simulations were performed for each turbine, reproducing operating conditions specified by the IEC 61400-2 power production DLC-group, including wind shear, yaw misalignment, and turbulence, as detailed in Table 3.

**Table 3.** IEC 61400-2 DLC 1.2 main set-up parameters.

| Parameter                                    | Value                        |
|--|------------------------------|
| Type of Evaluation                           | Fatigue/Ultimate             |
| Simulation Length                            | 600 s                        |
| Number of Simulations per W.S. and Yaw Angle | 3                            |
| Wind Speeds                                  | 2–20 m/s increments of 1 m/s |
| Yaw Angles                                   | 0/+8/−8 deg                  |
| Vertical Inflow Angle                        | 8 deg                        |
| Total Number of Simulations                  | 228                          |
| Total Simulated Time                         | 38 h                         |

These simulations had wind speeds between two and twenty meters per second in intervals of one meter per second following the standard and industry-accepted guidelines [12,55]. These design cases were representative of power production under normal wind conditions and would therefore be the most common within the turbine lifespan. Though DLCs are designed with structural certification in mind, they were used in this study to verify the productivity of the turbine, as they allowed us to simulate a normal power production scenario. Each simulation used a different turbulent speed (i.e., different turbulent wind field) in order to more realistically reproduce the conditions the turbine will encounter during operation and to avoid biases that might be introduced by a specific wind pattern.

As an additional verification, the convergence of power and annual energy production (AEP) was evaluated, as shown in Figure 7 and Table 4. This was important to evaluate to make sure that the predicted power curves could be considered independent from specific turbulence characteristics. The convergence of power was evaluated in terms of mean power per wind speed calculated with respect to the case using six turbulence speeds per wind speed (adding up to a total of one-hundred-fourteen simulations), as shown in Figure 7a. The analogous convergence of power standard deviation is shown in Figure 7b. Mean power was sufficiently well-predicted by using four turbulent speeds, with variations in mean power below 3% for all wind speeds. The standard deviations required more simulations to properly converge. As shown in Figure 7b, using five turbulent speeds ensured variations in Standard Deviation (STD) below 5% for all wind speeds.

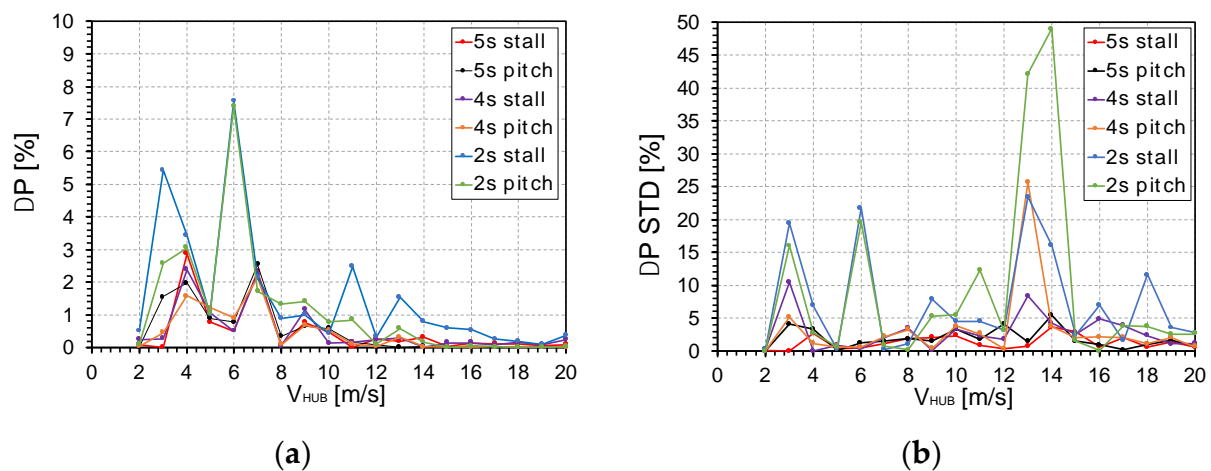


**Figure 7.** Relative error of power (a) and power standard deviation (b) per wind speed bin with respect to six speeds per wind speed value, using 5 (5 s), 4 (4 s), and 2 (2 s) turbulent speeds per wind speed.

**Table 4.** Statistical convergence of annual energy production (AEP).

| Speeds per WS          | 6     | 5     | 4     | 2     |
|------------------------|-------|-------|-------|-------|
| AEP stall              | 46.06 | 46.11 | 46.22 | 46.32 |
| $\Delta$ AEP (%) stall | -     | 0.117 | 0.345 | 0.575 |
| AEP pitch              | 52.55 | 52.69 | 52.65 | 52.53 |
| $\Delta$ AEP (%) pitch | -     | 0.251 | 0.176 | 0.040 |

AEP already showed strong convergence at two speeds per wind speed and is largely insensitive to increasing the number of speeds. This was in-line with the finding of Bortolotti et al. [56], who noted convergence on predicted fatigue loads and AEP using a small number of turbulent speeds. In conclusion, the minimum requirements of IEC 61400-2 in terms of turbulent speeds were able to guarantee the convergence of power and AEP in the present testcase.

## 5. Results

In this section, the results of the different design choices discussed so far are critically compared in order to let the reader evaluate their impact on the final performance.

### 5.1. Steady-State Performance

In order to evaluate general rotor performance, a steady-state performance comparison was carried out. Generator power as a function of windspeed is shown in Figure 8a. Both the stall and the pitch-regulated turbines were able to reach the desired output power of 50 kW. However, the pitch-regulated turbine reached rated power at 10 m/s wind speed, while rated power was not reached until 12 m/s in the stall-regulated turbine. For low

wind speeds of up to 8 m/s, the increased power output of the pitch-regulated turbine depended on the increased aerodynamic efficiency of this blade, caused by the fact that blade twist and pitch angle did not need to be compromised for effective stall regulation. From 9 m/s and above, the control strategy also had a direct effect, as the rotor speed was limited for the stall-regulated turbine in order to drive the blades to stall, as shown in Figure 8b and discussed in the previous section.

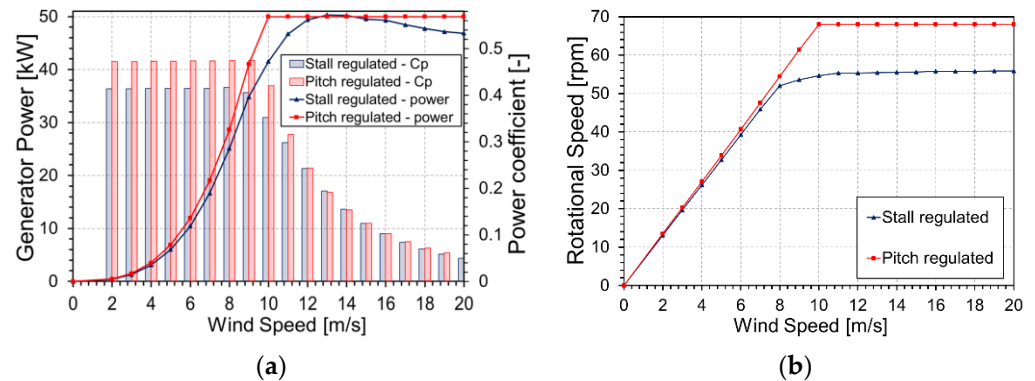


**Figure 8.** (a) Generator power and aerodynamic power coefficient; (b) rotational speed for pitch- and stall-regulated rotors in steady-state condition.

The observations made from a perusal of Figure 8a are confirmed in Figure 9, where the power coefficient is shown as a function of the tip-speed ratio: the compromises adopted for the stall-regulated turbine resulted in a generally lower power coefficient. Furthermore, the shape of the curve was very different, with the stall-regulated turbine presenting a pronounced peak in  $C_p$ , unlike the pitch-regulated turbine that could operate near peak- $C_p$  for a broad range of TSRs. It is also interesting to note that both turbines effectively operated in the area of the  $C_p$ -TSR curve that is on the left of the  $C_p$  peak. This was crucial, especially for a stall-regulated turbine, where tuning the shape of a  $C_p$ -TSR curve and forcing the rotor to operate in off-design conditions are the sole ways turbine control can be properly ensured.

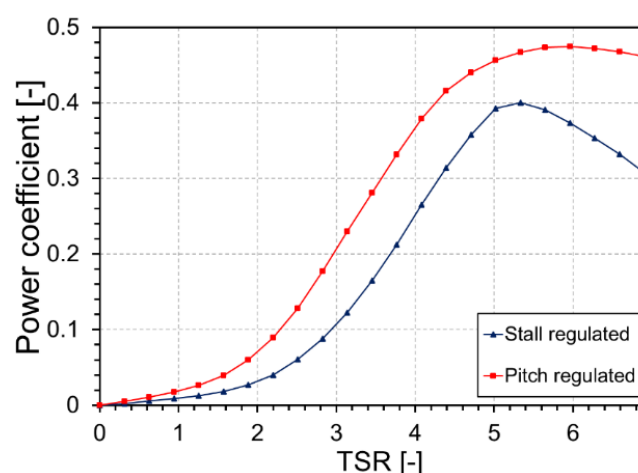


**Figure 9.** Aerodynamic power coefficient as a function of tip-speed ratio (TSR) in steady-state conditions.

### 5.2. Aerodynamic Performance

In this section, the aerodynamic performance in dynamic conditions is discussed. Figure 10 shows the generator power as a function of the wind speed for the two turbines in the conditions specified by IEC 61400-2 DLC 1.2 [12] and discussed in Section 4. The

error bars show the maximum and the minimum calculated values, while the filled areas represent the standard deviation. The analysis of the mean values shows that the power produced by the pitch-regulated turbine was higher than that generated by the stall-regulated turbine. This was largely because the pitch-regulated turbine was more efficient below the rated wind speed (Figure 8a). Furthermore, the standard deviation was generally lower for the pitch-controlled turbine at all wind speeds, and power output seemed to be better controlled, especially at high wind speeds. With their respective differences, these results show how the control systems of both turbines were able to adequately regulate the turbine in turbulent inflow conditions. The oscillation of the minimum power values for both turbines was due to the strong wind speed oscillations during turbulent simulations. This is in fact a key aspect of SWTs, whose installation contexts are often characterized by very turbulent winds.

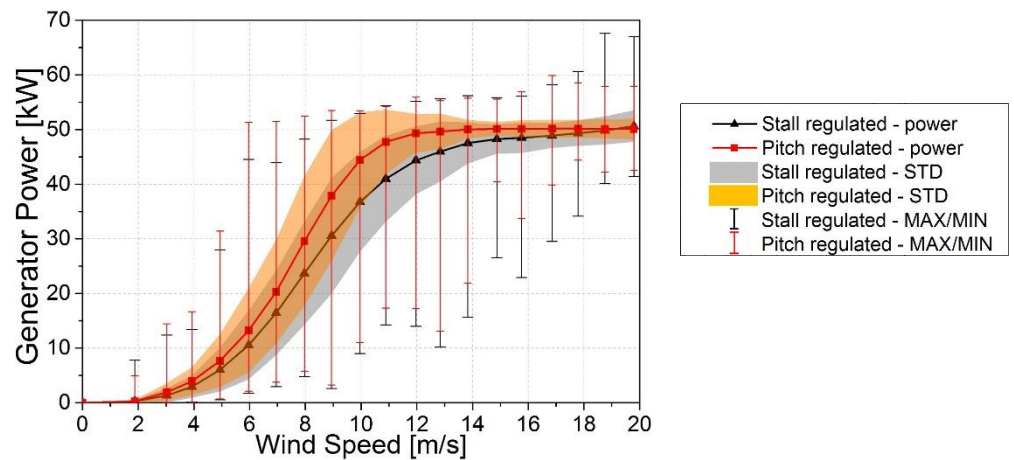


Figure 10. Generator power mean, standard deviation (shaded areas), and maxima and minima.

When comparing the power predicted in steady and dynamic conditions, some interesting considerations can be drawn. Figure 11a,b compares the power curves in steady and dynamic conditions for the pitch- and stall-regulated turbines. The effects of vertical up-flow, yaw-misalignment, and turbulence intensity can be globally evaluated.

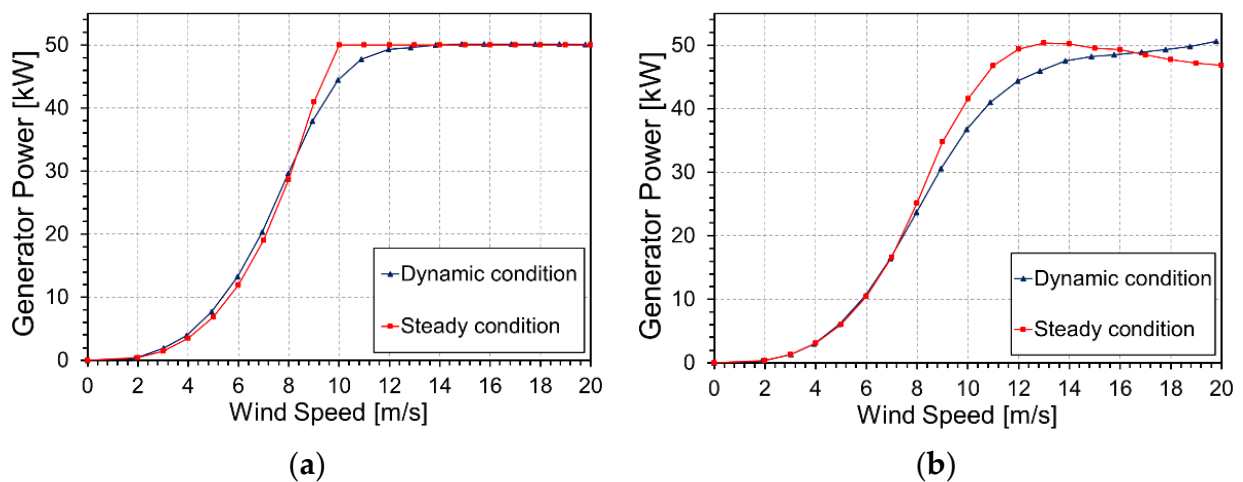
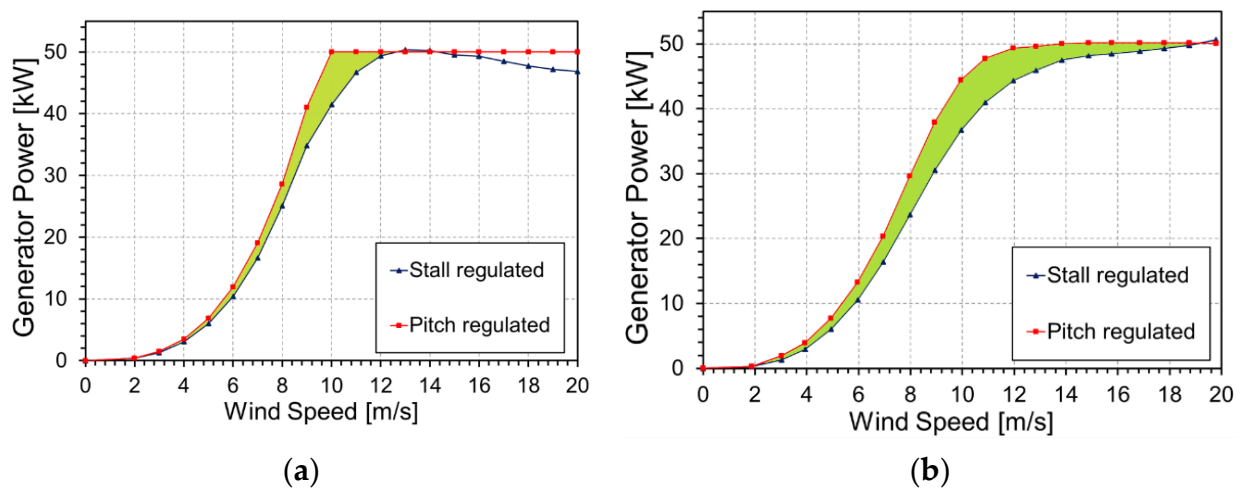


Figure 11. Power curves of the pitch- (a) and stall-controlled (b) variable speed concept.

For the pitch-regulated turbine, especially, there was a tendency to increase power output below rated power, while both the pitch- and stall-regulated turbines drastically

decreased power around the rated wind speed. This was mainly an effect of turbulence intensity, as many authors have shown [57–60], and underlines the importance of taking realistic operating conditions into account in the design process of a wind turbine (while in the past, this was discarded in many small wind turbines). For instance, in Figure 11b, one can notice how in turbulent flow conditions, the rated power was not reached until 20 m/s average wind speed; this could lead the designer to modify the turbine design, e.g., by compensating for this effect by reducing the fixed pitch angle.

By comparing the performance obtained in steady conditions with that in dynamic conditions, it can be noticed how the gap between the pitch-regulated and stall-regulated power curves widened in turbulent wind. This is very visible in Figure 12. Referring to this figure, the area between the curves in steady conditions was 27.06 kW\*m/s (Figure 12a) and 55.26 kW\*m/s in dynamic conditions (Figure 12b). This was a consequence of the flatter TSR– $C_p$  curve of the stall-regulated case, as shown above in Figure 9. For this reason, the pitch-regulated turbine was less sensitive to variations in TSR and could operate near peak  $C_p$  for longer time. This is again a consideration that was often unclear in the old generation of stall-regulated SWTs, and it seems to suggest that the real benefits of pitch regulation are higher than expectations and thus possibly able to compensate for the increased cost.



**Figure 12.** Power curves for the pitch- and stall-regulated turbines in steady conditions (a) and dynamic inflow conditions (b).

In above-rated flow speed operation, the stall-regulated turbine was able to self-regulate power output, as previously shown in Figure 7a. Unfortunately, as shown in Figure 13, the result was an increase in axial load for the stall-regulated rotor—more force was transferred into axial loading rather than into rotating the blade. In fact, as wind speed increased in the stall-regulated rotor, the force vector rotated downwind to decrease the torque component and increase the thrust component. Therefore, a potential advantage of pitch regulation over its stall counterpart is decreased peak axial loads, which decrease rotor structural requirements and may lower the risk of failure during high-wind events.

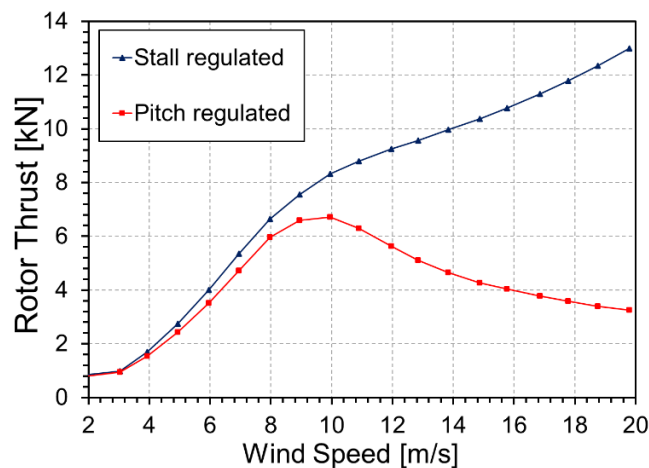


Figure 13. Average rotor thrust curves in dynamic conditions.

### 5.3. Annual Energy Production (AEP)

Differences in power delivery and efficiency discussed in the previous sections result in different annual energy production values. The AEP was calculated according to IEC 61400-2 standard turbine classes from the results of the dynamic simulations. A Weibull wind speed distribution with shape factor of 2 and an average value of 8.5 m/s was used to model sites of IEC wind class IIA, with medium wind speed and high turbulence intensities.

The results of AEP estimations are displayed in Figure 14. It can be noted that the energy capture was very low at low wind and high wind speeds, though for different reasons. At low wind speeds, a wind turbine cannot deliver enough power, while high wind speeds occur only for short times during a year.

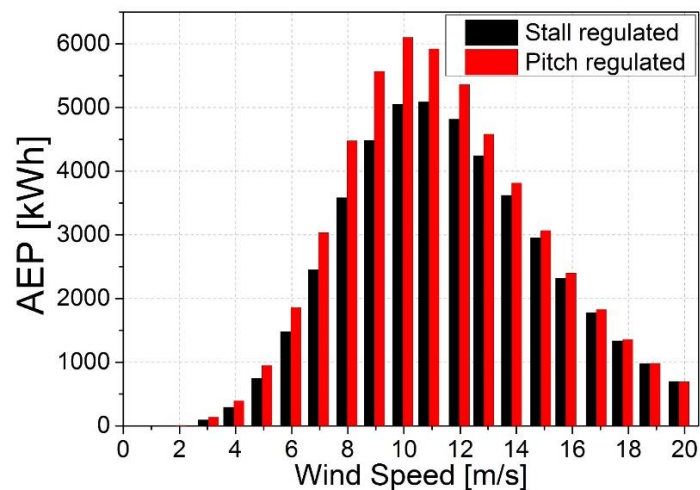


Figure 14. Annual energy production per wind average wind speed in dynamic conditions.

In the analyzed case study, the pitch-regulated turbine produced 12.36% more energy (kWh) annually than the same stall-regulated turbine. The annual energy production calculated for the stall-regulated turbine was 46.058 MWh/year, while the pitch-regulated turbine produced 52.554 MWh/year.

### 5.4. Results in the Time Domain

In order to do a comparative analysis between pitch and stall control strategies, it was also useful to look at time characteristics. The first reason for this is to show that the

controllers and simulation models worked properly. The second is to show the impact of the two control methods on power output, which also has an effect on global energy capture. Finally, the third is to get an impression of the power quality of the different controls.

In the following, below, above, and at around rated wind speed simulations are discussed, and the results for a 600 s time interval are shown. For the partial load time characteristics, an average wind speed of 7 m/s was selected. In this scenario, wind speed rarely reached its rated value, and power limiting did not occur. In this area, the main goal was to maximize energy harvesting.

In Figure 15a, the generated power is shown for the two turbines. In the 600 s time interval, the power of the pitch-regulated turbine was always slightly higher than that produced by the stall-regulated turbine, as was expected given the higher  $C_p$ . The power output was globally similar for the two turbines, as power regulation did not kick in until higher wind speeds were reached.

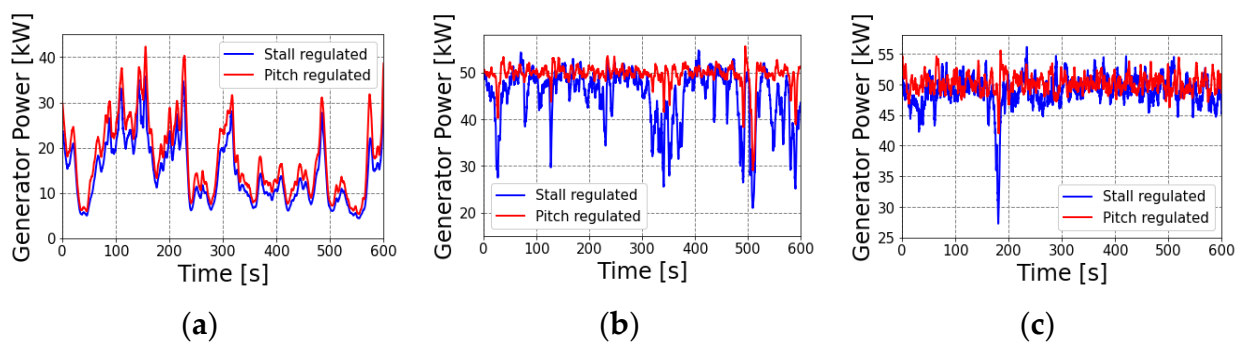


**Figure 15.** Generator power for a (a) 7 m/s average wind speed simulation, (b) a 12 m/s average wind speed simulation, and (c) a 16 m/s average wind speed simulation.

For the near rated wind speed time characteristics, an average wind speed of 12 m/s was selected. The main interest lies in the transitions from partial load to rated power and vice versa. In this area, a smooth transition between the power maximization and the power limiting was of interest. In Figure 15b, the power output for the two turbines at 12 m/s average wind speed is shown.

The stall-controlled variable-speed concept showed very steep power changes when entering and leaving region 3. While power overshoots were similar in magnitude for the two regulation concepts, power output dropped significantly as wind speed dropped below rated for the stall-regulated variant. When the turbine was operating at rated power, the blades were in partial or total stall; therefore, due to dynamic effects, power dropped significantly as the blade gradually exits stalled.

In Figure 15c, the behavior of the two different concepts at wind speeds above rated wind speed is shown; in particular, an average wind speed of 16 m/s was selected. At these wind speeds, there is always much more power in the wind than the wind turbine can handle. Therefore, the power output must be curtailed. Overall, the pitch-controlled turbine appeared to be able to regulate power more efficiently, although both control systems provided satisfactory results. As noted also when analyzing operation around rated wind speed, the generator power dropped significantly more on the stall-regulated turbine at the 180 s mark, an effect that could be again related to the stall state the blade is in.

Some interesting trends can also be inferred from the rotor speed of the same simulations at 7, 12, and 16 m/s shown in Figure 15; these trends are shown in Figure 16.

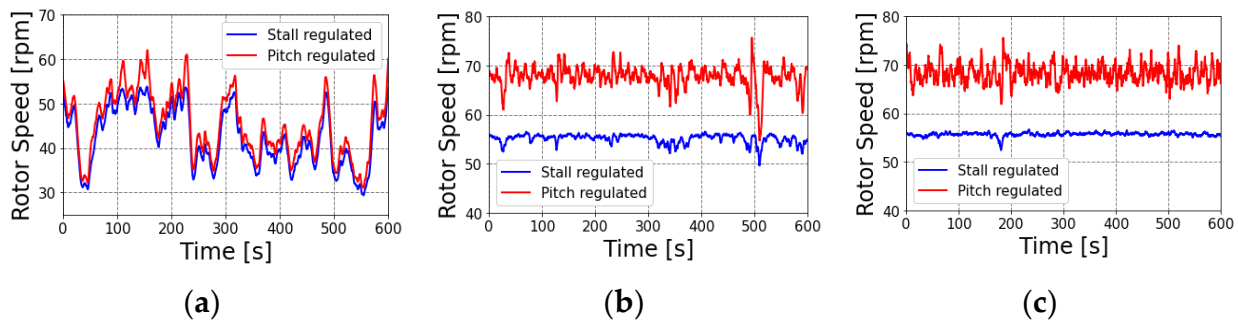


**Figure 16.** Generator speed for a (a) 7 m/s average wind speed simulation, (b) a 12 m/s average wind speed simulation, and (c) a 16 m/s average wind speed simulation. Results for the same simulations shown in Figure 15.

At 7 m/s, the two turbines behaved similarly, with the stall-regulated turbine producing more power and operating at a higher rotor speed. The stall-regulated turbine operated at a lower TSR, as intended and shown in Figure 9. At 12 and 16 m/s, the average rotor speed was higher for the pitch-regulated turbine and both turbines were operating at their nominal rotor speed, thus indicating that the controllers were performing as intended. It can be noted how the stall-regulated turbine was able to maintain a nearly constant rotor speed. The differences between control systems can be explained as follows: the pitch controller employed in this study maintained a constant torque above rated and regulated rotor speed and power through blade-pitch feathering. Thus, fluctuations in power were caused by variations in rotor speed and vice-versa. The stall controller, on the other hand, was set to operate in region 2.5 at a wind speed above rated (further details are discussed previously in Section 3.3), and controlled rotor speed at the expense of fluctuations in torque and power. Keeping rotor speed in check is very important for a stall controller because if rotor speed could increase, the turbine would increase its TSR and quickly accelerate out of control.

## 6. Conclusions

In this study, the design process of a 50 kW turbine from blade selection to performance assessment was used to show how modern engineering codes and recent tools for turbine control can be effectively used to design an efficient small wind turbine.

Focusing first on aerodynamic design, it must be noted that the intended final control strategy (i.e., pitch or stall control) needs to be defined early on in the design process because the resulting final blade shape may be significantly influenced by the choice. In the case of SWTs, it is preferable to use a family of airfoils that targets a high glide ratio with moderate lift coefficients, as this helps to increase blade chord and, hence, operating Reynolds number. Furthermore, although these effects are not fully understood and their inclusion in the design process is somewhat uncertain, it is very important to consider 3D-effects. Such phenomena play a key role in the inner parts of the blade and have been shown, as expected, to significantly influence the stall-regulation capabilities of an SWT. The presented guidelines and aerodynamic design procedure are general and can be applied to all turbine sizes, not only to SWTs. It must be noted, however, that when designing very large wind turbines (10–20 MW), pitch control is the undisputed choice and focus is placed mainly on structural loads. In fact, these rotors operate at extremely high Reynolds numbers, therefore achieving high peak aerodynamic performance almost effortlessly. On the other hand, structural optimization is extremely important to keep blade cost and weight down, as well as to guarantee robust blade design. For this class of rotors, a more integrated design procedure, focusing on loads in addition to aerodynamics and control in the initial stages of rotor design, should be considered.

Focusing on control, the study showed the basic approaches and methods to implement both pitch and stall control in small wind turbines. In this sense, even though existing books and reports very often only focus on the stationary power curve, it has been shown

here that in dynamic conditions, i.e., in a power-production DLC case from international design standards, the power curve of the turbine significantly changes, thus indicating the importance of accounting for such conditions in the design process and, especially, in the selection of the best control strategy.

For the stall-regulated turbine, an overall good level of performance was achieved. The peak aerodynamic power coefficient for the selected case study was around 0.4, which is in line with turbines of this class. When adopting a pitch regulation strategy, however, fewer compromises to the blade design have to be made in order to ensure good power regulation; in this case, no fixed blade pitch angle needed to be set, and the ideal blade twist distribution could be used. As a consequence, the aerodynamic power coefficient improved significantly, reaching a value of nearly 0.5, which is in line with most modern utility-scale turbines. Furthermore, rotor thrust continued to increase above rated wind speed for the stall-regulated turbine, as opposed to the trend observed when using pitch regulation. This points to the possibility that pitch regulation also has the added benefit of lowering axial blade loads. In this sense, this work has shown how the use of a modern, pitch-to-feather control strategy has the potential to significantly improve SWT performance through more effective power regulation and due to the fact that many compromises to the aerodynamic design can be avoided.

**Author Contributions:** Conceptualization, A.B. and F.P.; methodology, F.P.; software, A.N.; validation, A.N., F.P.; investigation, A.N.; data curation, A.N.; writing—original draft preparation, A.N.; writing—review and editing, F.P. and A.B.; supervision, A.B., G.F.; project administration, G.F.; All authors have read and agreed to the published version of the manuscript.

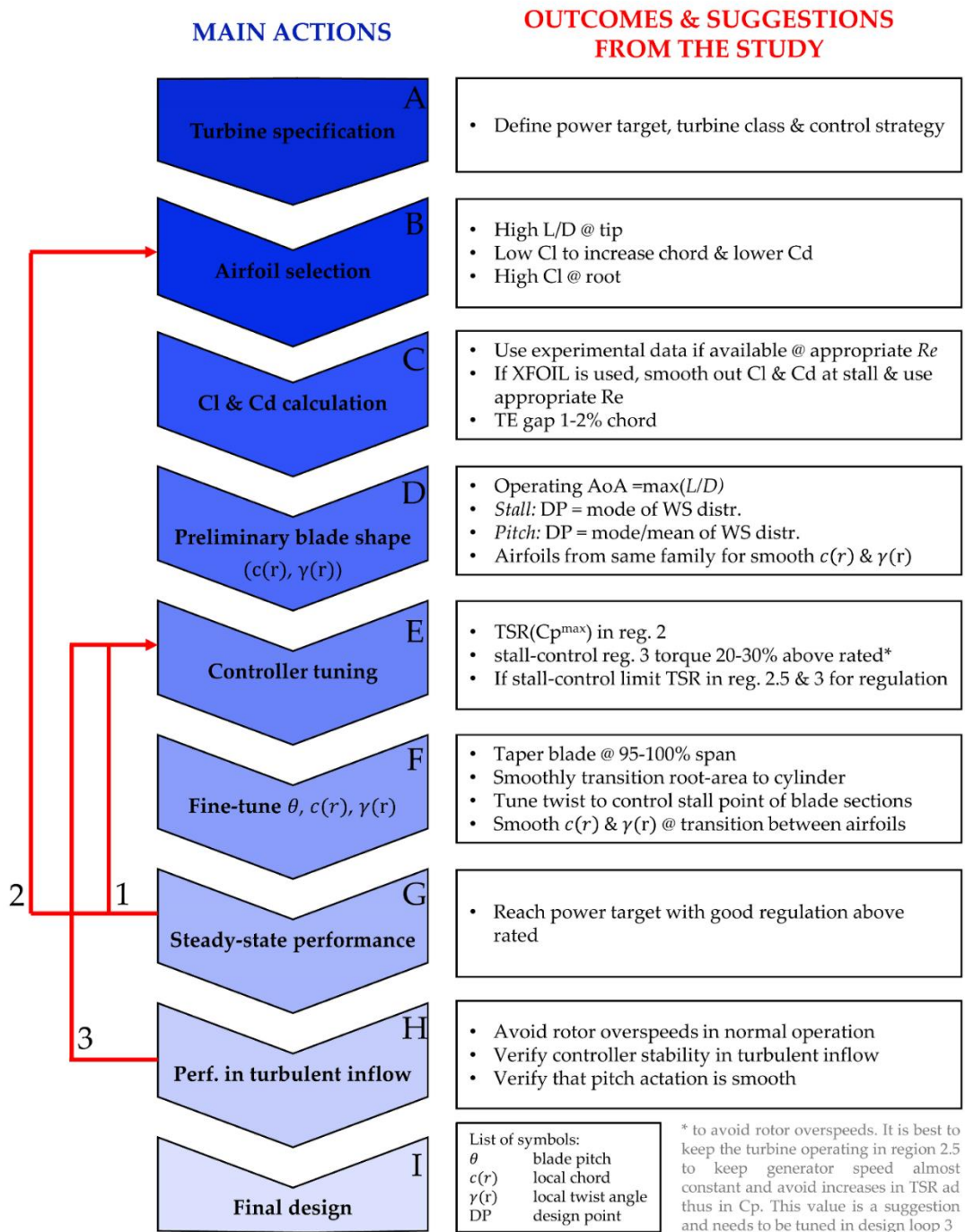
**Funding:** This research received no external funding.

**Informed Consent Statement:** Not applicable.

**Data Availability Statement:** Data available on request due to restrictions.

**Conflicts of Interest:** The authors declare no conflict of interest.

Appendix A



- Design loops 1&2 are necessary to understand if the chosen airfoil families and the controller parameters setting provide satisfactory performance. In many cases satisfactory performance can be reached trough loop 1 and fine-tuning blade shape in step F. If performance is still not satisfactory or stall regulation not as desired different airfoils must be chosen.
- The Final Design Loop allows for modifications to the ideal blade design in order to optimize the final aerodynamic performance. Trough steps E and F controller and blade can be fine-tuned in order to ensure good regulation and stability in turbulent inflow.

Figure A1. Conceptual scheme of the design phases for a SWT design procedure. Outcomes and suggestions from the study are reported for each phase.

## References

1. Veers, P.; Dykes, K.; Lantz, E.; Barth, S.; Bottasso, C.L.; Carlson, O.; Clifton, A.; Green, J.; Green, P.; Holttinen, H.; et al. Grand Challenges in the Science of Wind Energy. *Science* **2019**, *366*, eaau2027. [[CrossRef](#)] [[PubMed](#)]
2. Gardner, P.; Garrad, A.; Hansen, L.F.; Jamieson, P.; Morgan, C.; Murray, F.; Tindal, A. *Wind Energy—The Facts—Part 1: Technology*; EWEA: Brussels, Belgium, 2010.
3. Bukala, J.; Damaziak, K.; Kroszczynski, K.; Malachowski, J.; Szafranski, T.; Tomaszewski, M.; Karimi, H.R.; Jozwik, K.; Karczewski, M.; Sobczak, K. Small Wind Turbines: Specification, Design, and Economic Evaluation. In *Wind Turbines—Design, Control and Applications*; Aissaoui, A.G., Tahour, A., Eds.; InTech: London, UK, 2016; ISBN 978-953-51-2495-5.
4. Clausen, P.D.; Reynal, F.; Wood, D.H. Design, manufacture and testing of small wind turbine blades. In *Advances in Wind Turbine Blade Design and Materials*; Elsevier: Amsterdam, The Netherlands, 2013; pp. 413–431. ISBN 978-0-85709-426-1.
5. Tzen, E. Small Wind Turbines for on Grid and off Grid Applications. *IOP Conf. Ser. Earth Environ. Sci.* **2020**, *410*, 012047. [[CrossRef](#)]
6. Simic, Z.; Havelka, J.G.; Bozicevic Vrhovcak, M. Small Wind Turbines—A Unique Segment of the Wind Power Market. *Renew. Energy* **2013**, *50*, 1027–1036. [[CrossRef](#)]
7. EAWE Committees. Available online: <https://www.eawe.eu/organisation/committees/> (accessed on 13 January 2021).
8. Artal-Sevil, J.S.; Dufo, R.; Dominguez, J.A.; Bernal-Agustin, J.L. Small Wind Turbines in Smart Grids. Transformation of Electrical Machines in Permanent Magnet Synchronous Generators. In Proceedings of the 2018 Thirteenth International Conference on Ecological Vehicles and Renewable Energies (EVER), Monte-Carlo, Monaco, 10–12 April 2018; pp. 1–8.
9. James, F.M.; Jon, G.M.; Anthony, L.R. *Wind Energy Explained: Theory, Design and Application*, 2nd ed.; John Wiley & Sons: Hoboken, NJ, USA, 2010; ISBN 978-0-470-01500-1.
10. Burton, T. (Ed.) *Wind Energy Handbook*; John Wiley & Sons: Hoboken, NJ, USA, 2001; ISBN 978-0-471-48997-9.
11. Chaudhary, M.K.; Roy, A. Design & Optimization of a Small Wind Turbine Blade for Operation at Low Wind Speed. *World J. Eng.* **2015**, *12*, 83–94. [[CrossRef](#)]
12. IEC. IEC 61400-2. In *Wind Turbines—Part 2: Design Requirements for Small Wind Turbines*; IEC: Geneva, Switzerland, 2006.
13. Jacobson, R.; Meadors, M.; Jacobson, E.; Link, H. *Power Performance Test Report for the AOC 15/50 Wind Turbine*; NREL: Golden, CO, USA, 2003.
14. Eunice Energy Group (EEG). *EW16 THETIS—Wind Turbine 50kw*; Eunice Energy Group: Athens, Greece, 2020; p. 10.
15. Samani, A.E.; de Kooning, J.D.M.; Kayedpour, N.; Singh, N.; Vandeveld, L. The Impact of Pitch-To-Stall and Pitch-To-Feather Control on the Structural Loads and the Pitch Mechanism of a Wind Turbine. *Energies* **2020**, *13*, 4503. [[CrossRef](#)]
16. Small Wind Turbine Generators—Tozzi Green. Available online: [www.tozzinord.com](http://www.tozzinord.com) (accessed on 12 February 2021).
17. Drela, M. XFOIL: An Analysis and Design System for Low Reynolds Number Airfoils. In *Low Reynolds Number Aerodynamics*; Mueller, T.J., Ed.; Springer: Berlin/Heidelberg, Germany, 1989; Volume 54, pp. 1–12. ISBN 978-3-540-51884-6.
18. Tangler, J.L.; Somers, D.M. *NREL Airfoil Families for HAWTs*; NREL: Golden, CO, USA, 1995.
19. Battisti, L.; Zanne, L.; Castelli, M.R.; Bianchini, A.; Brighenti, A. A Generalized Method to Extend Airfoil Polars over the Full Range of Angles of Attack. *Renew. Energy* **2020**, *155*, 862–875. [[CrossRef](#)]
20. Drela, M.; Gilest, M.B. Viscous-Inviscid Analysis of Transonic and Low Reynolds Number Airfoils. *AIAA J.* **1987**, *25*, 1347–1355. [[CrossRef](#)]
21. OpenFAST. Available online: <https://github.com/OpenFAST> (accessed on 31 October 2019).
22. Jonkman, J.; Butterfield, S.; Musial, W.; Scott, G. *Definition of a 5-MW Reference Wind Turbine for Offshore System Development*; NREL/TP-500-38060; NREL: Golden, CO, USA, 2009; p. 947422.
23. Gaertner, E.; Rinker, J.; Sethuraman, L.; Zahle, F.; Anderson, B.; Barter, G.E.; Abbas, N.J.; Meng, F.; Bortolotti, P.; Skrzypinski, W.; et al. *IEA Wind TCP Task 37: Definition of the IEA 15-Megawatt Offshore Reference Wind Turbine*; NREL/TP-5000-75698; NREL: Golden, CO, USA, 2020; p. 1603478.
24. Jonkman, J.M.; Hayman, G.J.; Jonkman, B.J.; Damiani, R.R. *AeroDyn User's Guide and Theory Manual*; NREL: Golden, CO, USA, 2015.
25. Manwell, J.F.; McGowan, J.G.; Rogers, A.L. Aerodynamics of Wind Turbines. In *Wind Energy Explained: Theory, Design and Application*; John Wiley & Sons, Ltd: Chichester, UK, 2010; pp. 91–155. ISBN 978-1-119-99436-7.
26. Peter, J.S.; Richard, J.C. Wind Turbine Blade Design. *Energies* **2012**, *5*, 3425–3449.
27. Gasch, R.; Tvele, J. *Wind Power Plants Fundamentals, Design, Construction and Operation*, 2nd ed.; Springer: Berlin/Heidelberg, Germany, 2002; ISBN 978-3-642-22938-1.
28. Atlantic Orient AOC 15/50. Available online: <https://it.wind-turbine-models.com/turbines/2164-atlantic-orient-aoc-15-50> (accessed on 12 February 2021).
29. Smith, J.; Huskey, A.; Jager, D.; Hur, J. *Duration Test Report for the Entegrity EW50 Wind Turbine*; NREL: Golden, CO, USA, 2012.
30. E-3120 50kW Wind Turbine. Available online: [http://www.burnley.gov.uk/attachments/12\\_0055\\_Appendix\\_Endurance\\_E-3120\\_turbine\\_specifications.pdf](http://www.burnley.gov.uk/attachments/12_0055_Appendix_Endurance_E-3120_turbine_specifications.pdf) (accessed on 12 February 2021).
31. Mamadaminov, U.M. Review of Airfoil Structure for Wind Turbine Blades. *Or. Inst. Technol.* **2013**, *Energy Engineering I*, 1–8.
32. Fuglsang, P.; Bak, C. Development of the Risø wind turbine airfoils. *Wind Energy Int. J. Prog. Appl. Wind Power Convers. Technol.* **2004**, *7*, 145–162. [[CrossRef](#)]

33. Timmer, W.A.; Van Rooij, R.P.J.O.M. Summary of the Delft University Wind Turbine Dedicated Airfoils. *J. Sol. Energy Eng.* **2003**, *125*, 488–496. [[CrossRef](#)]
34. Somers, D.M. *Design and Experimental Results for the S805 Airfoil*; NREL: Golden, CO, USA, 1997.
35. Somers, D.M. *The S819, S820 and S821 Airfoils: October 1992–November 1993*; NREL: Golden, CO, USA, 2005.
36. Tangler, J.L.; NREL; Somers, D.M.; Airfoils, Inc. *Airfoils for Wind Turbine*; NREL: Golden, CO, USA, 1996.
37. Griffin, D.A.; Lynette, R. *Investigation of Aerodynamic Braking Devices for Wind Turbine Applications*; NREL: Golden, CO, USA, 1997.
38. Islam, M.R.; Bashar, L.B.; Saha, D.K.; Rafi, N. Comparison and Selection of Airfoils for Small Wind Turbine between NACA and NREL's S series Airfoil Families. *Int. J. Res. Electr. Electron. Commun. Eng.* **2019**, *4*, 1–12.
39. Ramsay, R.R.; Hoffmann, M.J.; Gregorek, G.M. *Effects of Grit Roughness and Pitch Oscillations on the S812 Airfoil: Airfoil Performance Report, Revised (12/99)*; Ohio State University: Columbus, OH, USA, 1999.
40. Ramsay, R.R.; Gregorek, G.M. *Effects of Grit Roughness and Pitch Oscillations on the S813 Airfoil: Airfoil Performance Report, Revised (12/99)*; Ohio State University: Columbus, OH, USA, 1996.
41. Somers, D.M.; Tangler, J.L. *Wind-Tunnel Test of the S814 Thick-Root Airfoil*; NREL: Golden, CO, USA, 1995.
42. Dal Monte, A.; de Betta, S.; Castelli, M.R.; Benini, E. Proposal for a coupled aerodynamic—Structural wind turbine blade optimization. *Compos. Struct.* **2017**, *159*, 144–156. [[CrossRef](#)]
43. Hansen, M.O.L. *Aerodynamics of Wind Turbines*, 2nd ed.; Earthscan: London, UK; Sterling, VA, USA, 2008; ISBN 978-1-84407-438-9.
44. Shen, W.Z.; Zhu, W.J.; Sørensen, J.N. Study of Tip Loss Corrections Using CFD Rotor Computations. *J. Phys. Conf. Ser.* **2014**, *555*, 012094. [[CrossRef](#)]
45. Himmelskamp, H. *Profiluntersuchungen an Einem Umlaufenden Propeller*; Report No 1945; Diss. Goettingen; Max-Planck-Inst. fuer Stroemungsforschung: Goettingen, Germany, 1950.
46. Hand, M.M.; Simms, D.A.; Fingersh, L.J.; Jager, D.W.; Cotrell, J.R.; Schreck, S.; Larwood, S.M. *Unsteady Aerodynamics Experiment Phase VI: Wind Tunnel Test Configurations and Available Data Campaigns*; NREL/TP-500-29955; NREL: Golden, CO, USA, 2001; p. 15000240.
47. Bak, C. Three-Dimensional Corrections of Airfoil Characteristics Based on Pressure Distributions. In Proceedings of the European Wind Energy Conference, Athens, Greece, 27 February–2 March 2006.
48. Abbas, N.J.; Wright, A.; Pao, L. An Update to the NREL Baseline Wind Turbine Controller. *Renew. Energy* **2020**, *17*, Preprint.
49. Mulders, S.P.; van Wingerden, J.W. Delft Research Controller: An open-source and community-driven wind turbine baseline controller. *J. Phys. Conf. Ser.* **2018**, *1037*, 032009. [[CrossRef](#)]
50. Muljadi, E.; Pierce, K.; Migliore, P. A conservative control strategy for variable-speed stall-regulated wind turbines. In Proceedings of the 2000 ASME Wind Energy Symposium, Reno, NV, USA, 10–13 January 2000.
51. Wright, A.D.; Fingersh, L.J. *Advanced Control Design for Wind Turbines Part I: Control Design, Implementation, and Initial Tests*; NREL: Golden, CO, USA, 2008.
52. ROSCO Tollbox, Version 1.0.0. GitHub Repository. GitHub: San Francisco, CA, USA, 2020.
53. Li, D.; Chen, C. Comparison of Energy Efficiency between Fixed-speed and Variable-speed Wind Turbines. *Energy Eng.* **2009**, *101*, 71–80. [[CrossRef](#)]
54. Jonkman, J.M.; Buhl, M.L., Jr. *FAST User's Guide*; NREL: Golden, CO, USA, 2005.
55. Hansen, M.H.; Thomsen, K.; Natarajan, A.; Barlas, A. Design Load Basis for Onshore Turbines. In *DTU Wind Energy Technical Report*; Department of Wind Energy: Roskilde, Denmark, 2015.
56. Bortolotti, P.; Canet, H.; Bottasso, C.L.; Loganathan, J. Performance of Non-Intrusive Uncertainty Quantification in the Aerose-voelastic Simulation of Wind Turbines. *Wind Energy Sci.* **2019**, *4*, 397–406. [[CrossRef](#)]
57. Bardala, L.M.; Sætrana, L.R. Influence of turbulence intensity on wind turbine power curves. *Energy Procedia* **2017**, *137*, 553–558. [[CrossRef](#)]
58. Kaiser, K.; Langreder, W.; Hohlen, H.; Højstrup, J. Turbulence Correction for Power Curves. In *Wind Energy*; Springer: Berlin/Heidelberg, Germany, 2007.
59. Albers, A.; Jakobi, T.; Rolf, R.; Stoltenjohannes, J. Influence of meteorological variables on measured wind turbine power curves. In Proceedings of the European Wind Energy Conference & Exhibition, Milan, Italy, 7–10 May 2007.
60. Wagner, R.; Courtney, M.; Larsen, T.J.; Paulsen, U.S. *Simulation of Shear and Turbulence Impact on Wind Turbine Performance*; Danmarks Tekniske Universitet, Risø Nationallaboratoriet for Bæredygtig Energi: Roskilde, Denmark, 2010.